Available online at www.sciencedirect.com

SCIENCE DIRECT®

Journal of Volcanology and Geothermal Research 139 (2005) 59–71

Journal of volcanology and geothermal research

www.elsevier.com/locate/jvolgeores

A numerical model for the dynamics of pyroclastic flows at Galeras Volcano, Colombia

G. Córdoba

Engineering Faculty, Universidad de Nariño, Colombia

Accepted 29 June 2004

Abstract

This paper presents a two-dimensional model for dilute pyroclastic flow dynamics that uses the compressible Navier–Stokes equation coupled with the Diffusion–Convection equation to take into account sedimentation. The model is applied to one of the slopes of Galeras Volcano to show: (1) the temperature evolution with the time; (2) dynamic pressure change; and (3) particle concentration along the computer domain from the eruption to the impact with a topographic barrier located more than 16 km from the source. Two initial solid volumetric fractions are modeled. For both cases, some of the structures located more distant than 10 km could survive, but in all cases the flow remains deadly. This paper shows that a dynamical model of pyroclastic flows can be implemented using personal computers.

Keywords: pyroclastic flow; model; numerical; finite element; hazard

1. Introduction

Galeras Volcano is regarded as one of the most active volcanoes in the world. Due to its geological characteristics, it is an explosive volcano with vulcanian type eruptions (Calvache et al., 1997), one of its hazards is the production of pyroclastic flows (Hurtado and Cortés, 1997). Geological studies performed by Calvache (1990), Calvache (1995) and Calvache et al. (1997) showed several occurrences of this hazard within its influence area. Investigations by Espinoza (1988) for historical activity of the last 500 years at Galeras Volcano from descriptions and photographs allowed Espinoza (1988) to deduce that pyroclastic flows occurred at least in five occasions, all of them without geological records (Banks et al., 1997). According to Banks et al. (1997), the volcano showed very small dilute surge-like flows during its active period of 1989. The fact that the historical pyroclastic flows have not left a geological record is evidence that such pyroclastic flows were composed mainly of a dilute cloud with a negligible basal part.

The last version of the Galeras Volcano hazard map (Hurtado and Cortés, 1997) establishes the run-out

E-mail address: gcordoba@udenar.edu.co.

0377-0273/$ - see front matter © 2004 Elsevier B.V. All rights reserved.
doi:10.1016/j.jvolgeores.2004.06.015

distance of the pyroclastic flows based on geological records. But from the risk assessment point of view, it would also be useful to know some of the dynamical parameters like temperature, particle concentration and dynamical pressure due to flow evolution in space and time. This would aide in estimating the devastation to structures or danger for people located in or near the flow path (Blong, 1984; Baxter et al., 1995; Valentine, 1998, e.g.).

Several analytical and numerical models based on fluid dynamics have been developed in order to describe the above parameter fields. These range from simple models which assume a non-transient, homogeneous, one-dimensional or radial flow (Sheridan, 1980; Bursik and Woods, 1991, 1996, e.g.) describing the main physical processes that occur from the column collapse to emplacement to the so-called supercomputer models (Valentine and Wohletz, 1989; Dobran and Neri, 1993; Neri and Macedonio, 1996a,b, e.g.) which model a tansient two-phase, compressible flow and a multiparticle solid phase (Neri and Macedonio, 1996a; Neri et al., 2001). The current development of personal computers enables the exploration of the possibility that a fluid dynamics model of pyroclastic flows can be implemented in a PC, including features which were beyond the scope for this kind of computers a few years ago. The proposed model focuses on the dilute turbulent companion ash cloud of a pyroclastic flow (see fig. 6.2 in Sparks et al., 1997) which allows one to make some assumptions in order to reduce the number of the equations and variables involved. This model could be considered as an intermediate between the abovementioned models, due to the fact that only one set of Navier–Stokes equations is used.

This model is applied to the channelized slope of the river basin of the Azufral River, which flows down from the active cone (located in the same direction) to the Guaitara River canyon, about 16 km away (Fig. 1). The main part of the Azufral river is confined within deep and nearly vertical walls which allows us to assume a 2D approach.

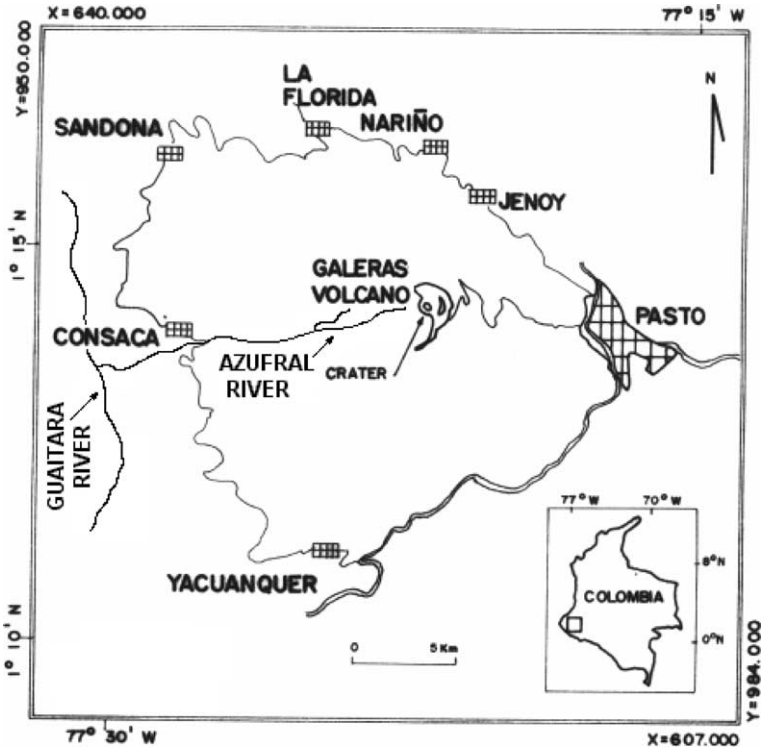

Fig. 1. Regional location of Galeras Volcano showing the Azufral River along which the proposed model is applied. Also, some towns under threat can be seen.

2. Mathematical model

From the point of view of physics, the dynamics of a pyroclastic flow is controlled by the mass, momentum and energy balance equations. It is a multiphase and multicomponent mixture, which carries gas (including water vapor), liquid drops of water and magma, clasts and fine ash. The pyroclastic flows at Galeras Volcano that occurred in the last 500 years were clearly dominated by fine ash as was pointed out above. As demonstrated by Sparks and Wilson (1976) and Neri and Macedonio (1996b), fine ash carried by some pyroclastic flows could comprise most of the flow in weight and volume. Thus for the model it is assumed that the dilute flow is composed of dry gas and a solid phase consisting (for simplicity) of one size spherical particles of 1 mm diameter. First, this size lets us assume a thermal equilibrium between particles and surrounding gas (Woods and Bursik, 1991). Additionally, for small particles, the Biot number, which relates the thermal conductivity with the heat transfer coefficient (Fan and Zhu, 1998), will be less than the unity, therefore only one equation is needed for the energy balance. Moreover, for Biot numbers less than 0.1, the temperature distribution in the solid can be considered uniform with a maximum error of 5% (Fan and Zhu, 1998).

Also, for very small particles, the two phases will move nearly at equal velocities (Stewart and Wendroff, 1984). Thus it will be assumed that the velocity of the solid phase will be the same as the gas phase and the material can be treated as a continuum with bulk flow properties (Freunt and Bursik, 1998) or the so-called two phase flow model with equal velocities (Stewart and Wendroff, 1984). In this way, only one set of Navier–Stokes equations will be used. However, it is considered that the change in the concentration of particles and its correspondent change in bulk density are a consequence of sedimentation by means of the Convection–Diffusion equation.

2.1. Government equations

The following equation system includes mass, momentum and energy conservation, coupled with the diffusion–convection equation, all equations expressed in the Einstein summation convention (Lai et al., 1974).

2.1.1. Mass

$$\frac{\partial \beta}{\partial t} + \frac{\partial (\beta u_j)}{\partial x_j} = -\frac{\partial (w_s \theta_s \rho_s)}{\partial x_j} \delta_{2j} \tag{1}$$

2.1.2. Momentum

$$\frac{\partial (\beta u_i)}{\partial t} + \frac{\partial (\beta u_i u_j)}{\partial x_j} = -\frac{\partial p}{\partial x_i} + (\beta - \rho_g) g_i + \frac{\partial \tau_{ij}}{\partial x_j} - \frac{\partial (w_s \theta_s \rho_s u_i)}{\partial x_j} \delta_{2j} \tag{2}$$

2.1.3. Energy

The energy equation expressed in its internal energy form:

$$\frac{\partial (\beta e)}{\partial t} + \frac{\partial (\beta e u_j)}{\partial x_j} = \frac{\partial}{\partial x_j} k_T \frac{\partial T}{\partial x_j} - p \frac{\partial u_j}{\partial x_j} + \frac{\partial \tau_{ij} u_j}{\partial x_i} \tag{3}$$

2.1.4. Convection–Diffusion equation

For small particles in a dilute suspension, and neglecting cohesive forces, the concentration of particles can be approximated by the convection–diffusion equation (Larock and Schamber, 1981; Chippada et al., 1993; Hermann et al., 1994):

$$\frac{\partial \beta \theta_s}{\partial t} + \frac{\partial \beta \theta_s u_j}{\partial x_j} = \frac{\partial}{\partial x_j} \mu_t \frac{\partial \theta_s}{\partial x_j} - \frac{\partial (\rho_s w_s \theta_s)}{\partial x_j} \delta_{2j} \tag{4}$$

where β = bulk density, u = velocity field, p = pressure, μ_t = turbulent eddy viscosity, g = gravity force, θ_s = volume fraction of solids, ρ_s = density of solids, ρ_g = gas phase density, w_s = characteristic settling velocity, k_T = bulk thermal conductivity, c_p = specific heat of the mixing, T = bulk temperature, δ_{ij} = Kroneker's delta and:

$$e = c_p T \tag{5}$$

2.2. Constitutive equations

The above equations system is closed by the following constitutive equations.

The Reynolds stress tensor τ_{ij} is:

$$\tau_{ij} = \mu\left(\frac{\partial u_i}{\partial x_j} + \frac{\partial u_j}{\partial x_i} - \frac{2}{3}\frac{\partial u_j}{\partial x_j}\delta_{ij}\right) - \overline{\beta u_i' u_j'} \quad (6)$$

The fluctuating part of the tensor can be approximated using the Boussinesq analogy (Wilcox, 1998):

$$-\overline{\beta u_i' u_j'} = -\mu_t\left(\frac{\partial u_i}{\partial x_j} + \frac{\partial u_j}{\partial x_i} - \frac{2}{3}\frac{\partial u_j}{\partial x_j}\delta_{ij}\right). \quad (7)$$

For a dilute flow, and neglecting particle interactions, the characteristic settling velocity can be approximated by (Sparks et al., 1997):

$$w_s = \left(\frac{4}{3}\frac{\rho_s g s}{C_d \beta}\right)^{\frac{1}{2}} \quad (8)$$

where: s=size of the pyroclasts and C_d is the Drag coefficient given by (Dobran and Neri, 1993):

$$C_d = \begin{cases} \frac{24}{Re_p}[1. + 0.15 Re_p^{0.687}], & \text{if } Re_p < 1000 \\ 0.44, & \text{if } Re_p \geq 1000 \end{cases}$$

where Re_p is the Reynolds number based on particle diameter.

By combining the effect of the temperature on viscosity through the Sutherland law (Zienkiewicz and Taylor, 1994) with the collisional viscosity (Wohletz, 1998), we arrive to the effective suspension viscosity:

$$\mu = \left(\frac{1.45 \times 10^{-6} T^{\frac{3}{2}}}{T + 110.}\right)(1. + \mathcal{M})^2 \quad (9)$$

where $\mathcal{M}$ is the mass ratio:

$$\mathcal{M} = \frac{\theta_s \rho_s}{(1 - \theta_s)\rho_g}.$$

The effect of turbulence is modeled through a Subgrid scale (SGS) effective viscosity (μ_t) using the Smagorinsky eddy viscosity (Wilcox, 1998):

$$\mu_t = \beta (C_s h)^2 \sqrt{\tau_{ij}\tau_{ij}} \quad (10)$$

where h is the size of the grid element and C_s is a constant related to the Kolmogorov constant, following Hartel (1996) $C_s \sim 0.17$.

2.3. Equations of state

As usual in this kind of models, we assume an ideal gas law:

$$p = \beta R T \quad (11)$$

where R is the gas constant of the mixture, $R = \frac{\Re}{M_g}$, $\Re$ being the universal gas constant and the molecular weigh of the gas is assumed as the same of the air M_g=28.964 kg/kg mol.

A bulk thermal conductivity is proposed, which relates the volumetric fractions of solids and gas with their respective thermal conductivities, as:

$$k_T = \theta_s k_s + (1. - \theta_s) k_g. \quad (12)$$

The bulk density can be estimated in a similar manner as (Stewart and Wendroff, 1984):

$$\beta = \theta_s \rho_s + (1 - \theta_s)\rho_g \quad (13)$$

where the gas density is calculated using the Boussinesq approach (Zienkiewicz and Taylor, 1994):

$$\rho_g = \frac{\rho_a}{1. + \theta(T - T_a)} \quad (14)$$

where ρ_a is the density of air at ambient temperature T_a, and θ is the thermal expansion coefficient.

The specific heat of the mixing is assumed here as the same as for the air and is related with temperature (Dobran and Neri, 1993):

$$C_p = (6. + 0.002T - 0.3 \times 10^{-6} T^2)\frac{4.18 \times 10^3}{M_g} \quad (15)$$

3. Solution procedure

3.1. Mass equation treatment

The mass equation is solved for pressure by manipulating Eq. (11). Deriving with time the state equation:

$$\frac{\partial p}{\partial t} = RT\frac{\partial \beta}{\partial t} + R\beta\frac{\partial T}{\partial t} \quad (16)$$

Then:

$$\frac{\partial \beta}{\partial t} = \frac{1}{RT}\frac{\partial p}{\partial t} - \frac{\beta}{T}\frac{\partial T}{\partial t}. \quad (17)$$

By assuming that the temporary change of the temperature is very small compared to the temperature itself, the last term in Eq. (17) can be eliminated and we arrive at:

$$\frac{\partial \beta}{\partial t} = \frac{1}{c^2}\frac{\partial p}{\partial t}. \quad (18)$$

Actually, the assumption in Eq. (18) implies that the flow is subsonic, specially if the value of c is taken as constant, and that no shock waves are present, which might not be true in a pyroclastic flow.

However, in our case c is the speed of sound of mixing which is defined by Dobran and Neri (1993) as:

$$c = \left(\frac{RT}{Y}\right)^{\frac{1}{2}}\left[Y + (1. - Y)\frac{\rho_g}{\rho_s}\right] \quad (19)$$

where Y is the mass fraction of gas in the two phase mixture:

$$Y = (1. - \theta_s)\frac{\rho_g}{\beta}. \quad (20)$$

The use of Eq. (19) and the Boussinesq approach (Eq. (14)) relaxes the approach outlined in Eq. (18), letting us have weak shock waves. But the mode is still limited to non-hypersonic velocities (Zienkiewicz and Taylor, 1994) due to our assumptions and the fact that we are solving the mass equation (Eq. (1)) for pressure. The use of this variable as the unknown does not work well in presence of strong shock waves (Codina et al., 1997). The sound speed inside a pyroclastic flow can be very slow and the flow could become supersonic. We will see this effect in the next part of this paper where the flow becomes supersonic at the jet. This occurs just at the entrance of the flow in the atmosphere, but with a maximum Mach number close to unity; and after that, most of the flow remains subsonic.

It is worth noting that by assuming a constant value for c in Eq. (19), which decouples the energy Eq. (3), the model is quite similar to those used in modeling powder snow avalanches (Hermann et al., 1994; Keller, 1996, e.g.). In the same way, the model could be used for modeling cool pyroclastic flows.

3.2. Biot number checking

Due to the fact that a single particle size has been assumed, the Biot number (Fan and Zhu, 1998) can be approached from:

$$B_i = \frac{h_T}{k_p/s} \quad (21)$$

where: B_i = Biot number, h_T = heat transfer coefficient between particles and surrounding gas, k_p = particle thermal conductivity, s = particle diameter, assumed here as 1 mm.

The heat transfer coefficient h_T can be related to the Nusslet number:

$$N_u = \frac{h_T s}{k_g} \quad (22)$$

where k_g is the gas thermal conductivity.

The Nusslet number is also related to the Prandtl number and Reynolds number based on particle diameter and the velocity difference between particles and gas (Re_{gp}). According to Gunn (1978), this number can be approached as $N_u = (2+5\theta_s^2)$ due to an equal velocity model that has been assumed. For both cases of θ_s, $N_u \sim 2.0$, and with the proposed initial conditions, from Eq. (22), we arrive at $h_T = 100$ and thus from Eq. (21), $B_i = 0.045 < 0.1$. Thus the assumption of one equation for energy balance is justified.

3.3. Numerical approach

Once the partial differential equation system has been re-written in this way, it is then discretized and solved using the Finite Element Method (Taylor and Hughes, 1981; Zienkiewicz and Taylor, 1994) and implemented using the trademark FASTFLO, a tool for finite element method users developed by the Numerical Algorithm Group (NAG).

Due to the strong non-linearity and the anticipated instabilities (Betts and Sayma, 1993; Chippada et al., 1993) we use the Operator Splitting Algorithm (Glowinski and Pironnean, 1992) and two types of artificial viscosities at the same time, in order to avoid

the negative diffusivity induced by an Euler approach: a Lapidus like diffusivity (Zienkiewicz and Taylor, 1994):

$$k_{ij} = C_{\mathrm{Lap}} h^2 \frac{||u_i u_j||}{||u||} \tag{23}$$

where C_{Lap} is the Lapidus coefficient, and the balancing tensor diffusivity (BTD) (Eguchi and Yagawa, 1988):

$$k_{ij} = \frac{\Delta t}{2} u_i u_i \tag{24}$$

where the time increment Δt is computed, each time step is followed to ensure stability, obtaining the minimum (Zienkiewicz and Codina, 1993; Zienkiewicz and Taylor, 1994):

$$\Delta t = \frac{h}{|u| + c}\left(\sqrt{\frac{1}{Pe^2} + \frac{1}{3}} - \frac{1}{Pe}\right) \tag{25}$$

where Pe is the Peclet number, a Reynolds-like number based on size of the grid element (h):

$$Pe = \frac{h|u|}{2\mu} \tag{26}$$

3.3.1. The mesh

Because the model is applied to the Azufral River basin which is within a channelized slope, a two-dimensional approach is chosen. The 2D domain was discretized using a six node isoparametric triangle as the basic element (Fig. 2). The total mesh has about 30.000 triangles with a concentration of cells at interesting points like the crater borders or strong changes in slope. The minimum size of the element was chosen according to a sensitivity test, performed below, and was taken as 11 m. Fig. 2 shows the Azufral River at the bottom (ground), and the crater at the lower left corner. The lowest part to the right hand side is the point at which the Azufral River reaches the Guaitara River canyon, this river flows down in a direction toward the reader. The wall of the Guaitara River canyon follows to the right reaching the numerical boundaries. The top of the mesh is located 6.1 km above sea level.

3.3.2. Boundary conditions

As in all numerical approaches, it is necessary to define proper boundary conditions at the borders of the grid. This is a critical matter because choosing wrong boundary conditions could cause the problem to be ill-posed. At present there are clear techniques to improve proper bc's either for incompressible flows or for compressible flows, according to the Mach number (M) of the flow (Vazquez et al., 1999):

- If $M<1$: two conditions at inlet (u, T), one condition at the outlet (ρ or p);
- If $M>1$: three conditions at inlet (u, T, ρ or p), none at outlet.

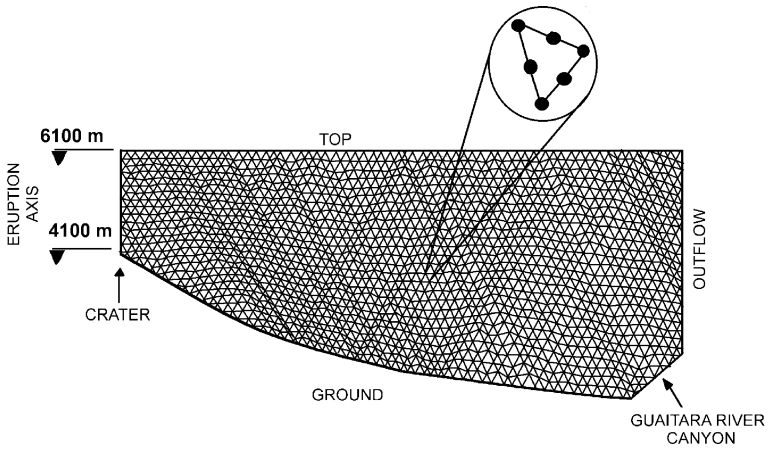

Fig. 2. Finite element mesh which has about 30.000 six node isoparametric triangles. The mesh is refined at areas and points with a strong change in slope. The minimum size of the element, shown at the upper part of the figure, is 11 m. The inflow is located in the crater at the lower left corner.

The modeling of pyroclastic flows from the beginning of the eruption to its emplacement, implying that the model is located just in the middle of the above conditions: part of the flow could be supersonic and part of it will be subsonic, as in our case. At present, intensive research is being done in order to handle both compressible and incompressible cases (see for example Zienkiewicz and Codina, 1993; Codina et al., 1997; Vazquez et al., 1999).

In the proposed model, the next conditions are imposed according to Fig. 2: At the ground, a Dirichlet condition for velocity is imposed with a value of zero, which means a non-slip condition. For the other variables, Newman conditions are imposed (zero flux). Additionally, neither mass nor heat transfer is allowed.

At the outlet there is a zero stress condition (σ_{xy}=0.0). At the top, a zero stress condition and a free vertical velocity. At the axis of the eruption, a free vertical velocity. At the crater, the inlet conditions (see next section). In addition to the above conditions it was necessary to impose two points with known pressure and temperature (defined with its ambient values) at upper left and right corners of the mesh in order to reach convergence and avoid some non-physical reflexions.

3.3.3. Initial conditions

By neglecting particle segregation, which could play an important role in a collapsing fountain (R.S.J. Sparks, 2002, personal comm.), two constant volumetric solid fractions of θ_s=0.005 and θ_s=0.01 at inflow are used. This means from Eq. (13) an initial bulk density of 12.7 kg/m^3 is determined in the first case. This initial density is within the range of most collapsing columns, which is between 8 and 18 kg/m^3 according to Sparks et al. (1997). For the second case, an initial bulk density of 24.2 kg/m^3 is obtained. The chosen values for θ_s correspond to eruptions A (approximately) and B in Dobran and Neri (1993). Finally, the initial conditions at the vent and in the inner part of the grid (ambient conditions) are as follows:

V_v = Turbulent profile with mean velocity $\bar{V}$=100 m/s
T_v = 1200 K
T_a = 288 K
θ_{sv} = 0.01 and 0.005
R_v = 150 m
ρ_a = 1.22 kg/m^3
ρ_s = 2.300 kg/m^3
k_g = 0.05 W/m K
k_s = 2.2 W/m K
s = 1 mm
$\dot{m}$ = 8.2×10^7 kg/s for θ_s=0.01
$\dot{m}$ = 4.2×10^7 kg/s for θ_s=0.005.

Subscripts v and a represent respectively conditions at vent and ambient (R_v is the vent radius).

The turbulent profile was defined according to hydraulics:

$$v = \overline{V}\left[\sqrt{f}\left(2\log_{10}\frac{y}{R_v} + 1.32\right) + 1.\right] \tag{27}$$

where f=friction factor of the conduit and y=distance from wall of the conduit.

The friction factor is calculated from the Colebrook and White formula:

$$\frac{1}{\sqrt{f}} = -2\log_{10}\left[\frac{k_s}{3.7d} + \frac{2.51}{Re_v\sqrt{f}}\right] \tag{28}$$

where K_s=roughness of the wall assumed as 0.5 m, Re_v=Reynolds number at inlet based on vent diameter and mean velocity, and d=conduit diameter.

From the above initial conditions and using Eqs. 13, 14, 17 and 19 the Mach number for each volumetric fraction of solids is calculated as: M=1.3 for θ_s=0.01 and M=0.92 for θ_s=0.005. Then, according to these initial conditions, in some cases the flow reaches the supersonic field but it always remains non-hypersonic.

4. Results

Basically two eruptions were simulated, with the above initial conditions, and three more were done as a sensitivity test with different grid sizes.

The model was implemented in a PC using an Intel™ PentiumIV processor with 1.6 GHz running under Linux OS. The CPU time was about 10 days, which might be acceptable computing time for the PC's.

The temporal evolution of the temperature for both cases is shown in Fig. 3, at 150 s and at 400 s for

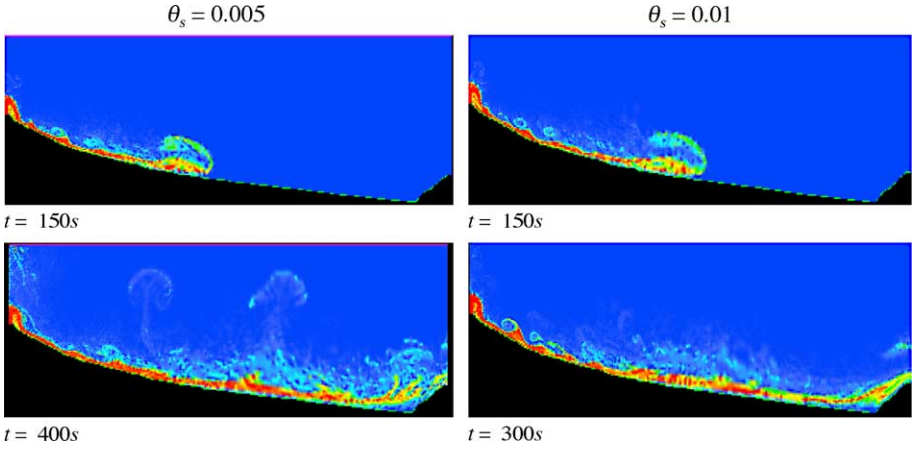

Fig. 3. Two stages of temperature evolution for each case modeled. After 150 s, the simulation shows several eddies, also the flow reaches the middle of the path. For an initial solid volumetric fraction of $\theta_s = 0.005$ the flow becomes more buoyant and plumes appear after 400 s. In despite of the loss of material due to buoyancy, in both cases the flow reaches and surmounts the Guaitara River canyon but at different times, the case $\theta_s = 0.01$ is faster.

$\theta_s = 0.005$ and 300 s for $\theta_s = 0.01$ after the beginning or the eruption. Note that for $\theta_s = 0.005$ the flow needs more time to reach the topographical barrier because it descends at a lower velocity than the more concentrated flow. The flow becomes more buoyant than in the case of $\theta_s = 0.01$ and consequently thermals form at around 400 s after the eruption. The barrier is reached by the flow with a temperature of about 650 K, which means that all types of life could become totally extinct and buildings could be at least burned along its path. Additionally, note that this model successfully shows the pulsating behavior of the collapsing column and the front of the pyroclastic flow is reached by backward flow coming at greater velocities as was noted by Neri and Macedonio (1996b).

From a hazard point of view, it is also important to understand at least two other fields: (1) particle concentration, which can indicate the possibility of motality (according to Baxter et al., 1995, a concentration equal or grater than 0.1 kg/m^3 could kill people) or bury structures due to the high concentration of solids carried by the flow; and (2) dynamic overpressure ($p = 1/2\beta u^2$). Fig. 4 shows the results of the simulation for (a) particle concentration, (b) dynamical pressure and (c) Mach number, for $\theta_s = 0.005$ and $\theta_s = 0.01$, all of them derived at 240 s after eruption. They show the field of interest versus the altitude from the ground. Each graphic gives results at three distances from vent, namely 2 km (solid line), 6 km (long-dashed line) and 10 km (short dashed line).

4.1. Particle concentration

For an initial volumetric fraction of solids of $\theta_s = 0.005$ the maximum concentration of particles is around 12 kg/m^3 at the base of the pyroclastic flow and close to the vent (2 km), the threshold for human survival (HST = 0.1 kg/m^3) is located at an altitude more than 450 m from the ground. At 6 km away from the crater the maximum concentration is about 5 kg/m^3 at ground level and the 0.1 kg/m^3 is at about 1000 m altitude, which shows the expansion of the flow. At 10 km distance, the head of the flow has formed. It has lost most of its density due to turbulent expansion, sedimentation and thermal buoyancy. Here the maximum concentration is about 1 kg/m^3 at ground level and the HST is at more altitude than 1650 m. At this stage (not shown in Fig. 4), the front of the flow is located at 13 km from the vent with a concentration of particles above the HST. The flow remains lethal along the path and structures could be buried at a distance of 6 km away from the crater. Buildings could be at minimum impregnated by ash at even further distances.

For $\theta_s = 0.01$, the results at 2 km distance shows that the maximum concentration is about 23 kg/m^3 at

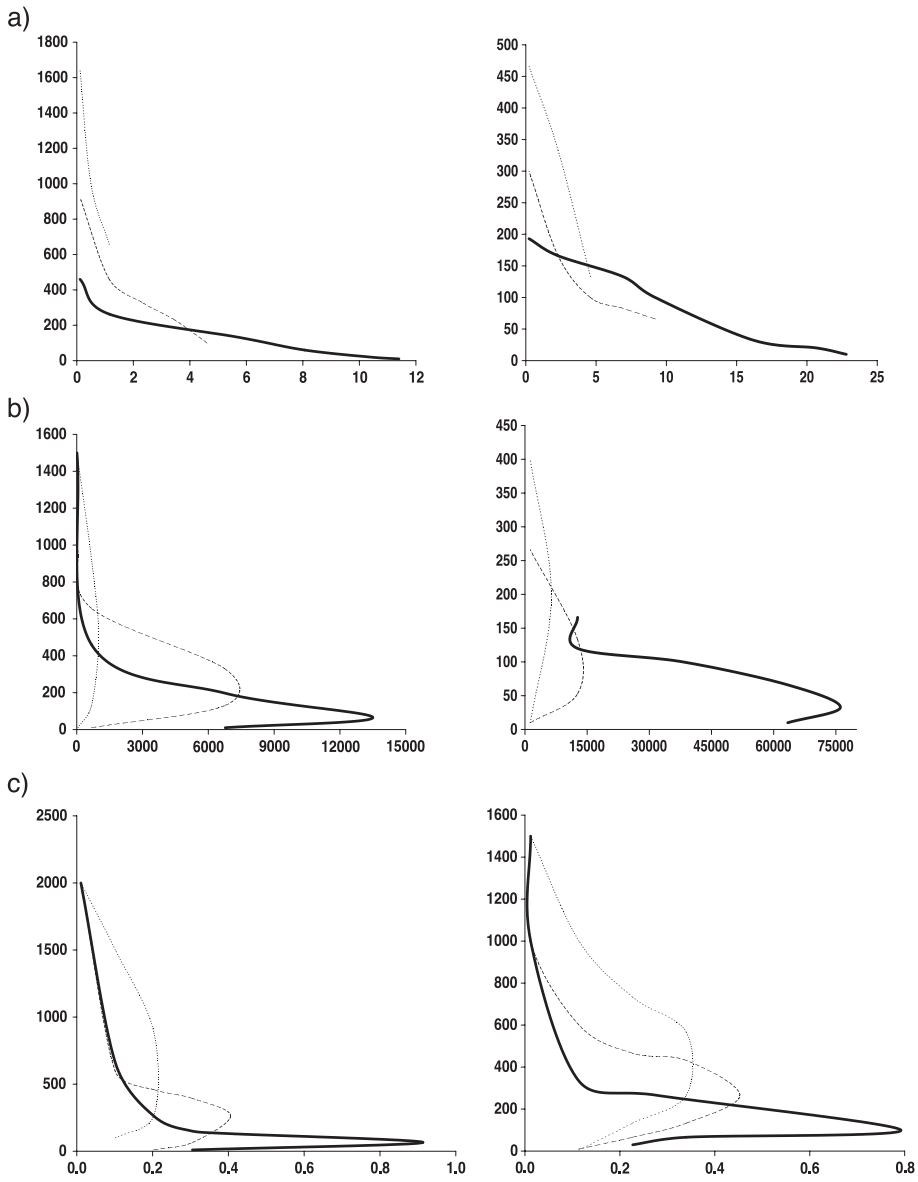

Fig. 4. Vertical distribution of (a) particle concentration, (b) dynamical pressure and (c) Mach number after 240 s from the eruption for θ_s= 0.01 and θ_s= 0.005. Curves correspond to distances of 2 km from the crater (solid line), 6 km distance (long dashed line) and 10 km from the crater (short dashed line). The vertical axis shows the altitude above the ground level. Note the expansion of the flow in figures (b) and (c) by watching the maximum peak in the dynamical pressure and the Mach number, which are placed at the highest altitude as flow advance.

ground level and that the HST is located about 200 m altitude. At 6 km, the maximum is about 10 kg/m^3 at ground level and the HST is at an altitude of more than 300 m. Finally, at a distance of 10 km the maximum concentration is about 5 kg/m^3 at the base of the flow and the HST is located at 500 m altitude. The front of the flow just reaches the topographical barrier with concentrations about 2 kg/m^3 (not shown in Fig. 4). Under this initial volumetric fraction of solids the flow is also faster than the other one. Of course, the flow is more dangerous, and it could bury structures along all its path and also it remains lethal

in the distance between the vent and the Guaitara River canyon.

4.2. Dynamical pressure

Despite the strong damage produced by the high temperatures of most pyroclastic flows, the dynamical overpressure might produce the most noticeable destruction among all the effects of a pyroclastic flow impact. A dynamical overpressure of 10 kPa is considered as the human survival threshold (HST) according to Taniguchi and Suzuki-Kamada (1993). This overpressure is sufficient to "blow off" the human body. A detailed description of the effect of the volcanic dynamical overpressure on structures has been done by Valentine (1998), from which it is only mentioned the case of little damage for dynamical overpressures around 7–14 kPa and total demolition for dynamical pressures of about 100 kPa.

As we can see in Fig. 4b, for an initial volumetric fraction of solids of θ_s=0.005, the maximum overpressure reached is around 14 kPa at a distance of 2 km away from the vent, and located more than 60 m altitude from ground. However, at about 10 m altitude the dynamical overpressure does not reach 7 kPa, there is a small or reparable damage could be expected in lower floors of high structures. Far away from the vent (more than 6 km) the dynamical overpressure does not reach 7 kPa. Thus, the HST is reached only at closer distances from the vent.

For θ_s=0.01, the maximum dynamical overpressure is about 80 kPa at 2 km and 30 m altitude (but 60 kPa at 10 m). Six kilometers away, this maximum falls to around 14 kPa at 50 m height. From this distance (really 7 km) the highest dynamical overpressure remains around 1.4 kPa.

In summary, strong damage or total destruction could be expected for structures located at distances up to 6 km, and little damage from 6 to 10 km distance. Buildings located more than 10 km away could survive without serious structural damage.

Note that for both of the simulated cases noticeable structural damage affects buildings located as close as 6 km from the vent. It is worth mentioning that the dynamical overpressure at altitude close to ground is lower than the damage threshold (7 kPa according to Valentine, 1998) for θ_s=0.005. This could explain the reason why in some reported cases the destruction was focused on the upper parts of buildings, leaving the lower parts standing (Sparks et al., 2002, e.g.): overpressure close to ground might not be sufficient to demolish the structure in contrast to the high dynamical overpressure at greater altitude, combined with the shear produced by debris or pumice impacts.

4.3. Mach number

Due to the mathematical model proposed that assumes low Mach numbers, part c of Fig. 4 shows the behavior of possible shocks. At the vent (not shown in the figure) the Mach number is 1.2. After the column collapse, the flow accelerates and at the first strong change in slope, just before 2 km distance, the maximum Mach number is around 1.0 for both cases, but at different altitudes. For θ_s=0.005 this maximum is at 70 m altitude and for θ_s=0.01 is at 100 m altitude. At the base of the flow, where a non-slip condition was assumed as a boundary condition, the Mach number falls to zero. This shows that the weak shocks assumed by the mathematical model have been conserved along the path in both simulated cases.

4.4. Sensitivity test

In order to test the numerical accuracy of the results, three trials with different minimum element sizes were carried out: 11, 7 and 5 m. Due to time constraints of the CPU, all of them were carried out using a mesh which considers a 4 km distance using the same initial and boundary conditions as the main simulations. Fig. 5 shows the trials for (a) 11 m and (b) 7 m. The advance in both cases are the same, but as expected, more eddies are resolved in the finer grid. Using 5 m as a minimum size of the element, no convergence was reached. After about~20 s, a "hot point" appeared and it led to divergence. Perhaps the reason for this could be explained either by the propagation of a rounding error added to a non-physical location of shocks due to the use of a non-conservative form of the energy equation (Codina et al., 1997; Vazquez et al., 1999). Alternatively, it could be due to the difficulty in improving proper boundary conditions. The CPU time for the cases shown in Fig. 5 was 5 days for a minimum element size of 11 m and

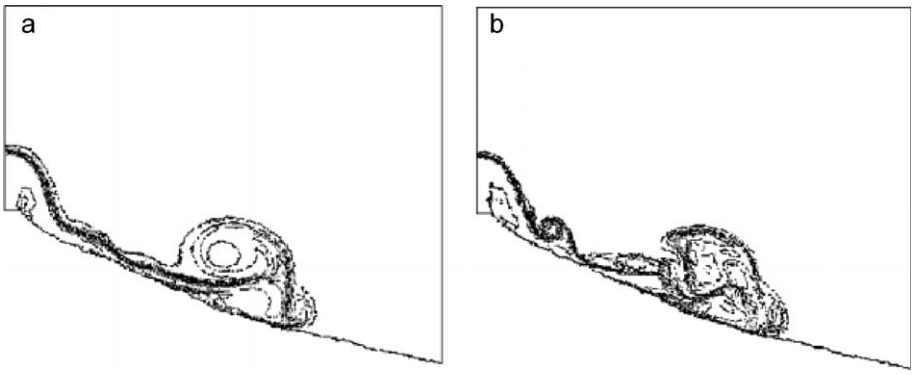

Fig. 5. Sensitivity test for (a) a minimum grid size of 11 m, and (b) a minimum size of 7 m showing the particle concentration contour lines. Note that more eddies are resolved using a smaller size of grid. In both cases, 4 km length of the river is shown. The CPU time for 11 m was 5 days but 9 days for the second case, making unacceptable the computing time for the entire mesh, which takes into account the 16 km of distance.

9 days for a minimum size of 7 m. Due to the principal simulations being carried over a distance of 16 km, it was decided to perform the simulations over all the mesh by using a minimum size of 11 m that allows an available computing time without losing too much accuracy.

5. Conclusions and outlook

This paper proposes a model for pyroclastic flows at Galeras Volcano. The model takes into account the dynamic behavior of the dilute part of the flow that has been implemented in a PC. The pyroclastic flow modeled here could be regarded as a pyroclastic flow of high speed whose front advances as an expanded turbulent head followed by a highly concentrated body, as it has been described by Sparks et al. (1997). Two main simulations have been performed for initial volumetric fraction of solids θ_s=0.05 and θ_s=0.01. In despite of all the assumptions, the simulations produce some data that can be used for hazard mapping such as the fields of temperature, particle concentration and dynamical overpressure.

From a human point of view, both of the simulated flows remain deadly along their entire paths. Firstly, because the temperature remains higher than 600 K, and the solid concentration is always more than 0.1 kg/m^3. Despite this, the dynamic overpressure probably is not deadly for approximately 10 km distance. Other factors ensure that people reached by the flow will be at least buried and burned (dead and impregnated by ash?).

From the structural point of view, buildings located as close as 6 km could be destroyed due to dynamic over pressures above 5 Pa. Structures located farther than 10 km might remain standing and reparable, mainly those seismically designed. However, all buildings might be burned or at least could suffer fires.

The above reasons classify this hazard along the Azufral River with a severity of 5 and a vulnerability of 1 for all structures within a distance of 6 km, and a severity of 4 at further distances.

In both simulated cases, the flows reach and surmount the topographical barrier formed by the Guaitara River canyon, seemingly threatening locations which at present have not been placed in the current Galeras Volcano Hazard Map (Hurtado and Cortés, 1997). Nevertheless, in this paper a friction factor has not been implemented, therefore the roughness and winding of the channel has been neglected. Also, the two-dimensional approach lets the flow maintain its energy for more time and the impact on the topographical barrier would spread the flow in a 3D feature. All the above considerations indicate that it is necessary to be careful in prediction of run-out distance because the model still is not capable of stopping the flow, at least in its most dilute part. An area for future study improvement is a stopping mechanism to halt the flow. Finally, a very

dilute flow could show hazardous behavior without leaving a geological record.

The CPU time required (10 days) can be considered acceptable for the magnitude of the problem, taking into account that the model was implemented on a home PC. Of course, parallel computation could be the best computing tool to simulate the dynamical behavior of a pyroclastic flow, but this kind of computational machine is beyond the scope of possibility for most places threatened by explosive volcanism, at least within a short-term future. At present, the model does not take into account the dense suspension at the basal part of the flow, the winding path of the river, and friction. These deficiencies in the model and the 2D approach could produce an excessive velocity calculation along the path. Also, the fact that the simulation diverged as the mesh was refined warns us that extreme caution should be taken with the results shown here.

In the near future, model improvements should: ensure convergence and stability for all grid sizes, circumvent the dilute flow constraint and account for the basal avalanche. The inclusion of a friction factor, the addition of the water vapor phase or multi-component solid phase through the Diffusion–Convection equation, and the development of features which do not increment the CPU time by much will allow the use of PCs in this type of flow analysis. Also, it is necessary to include more realistic initial conditions at the Galera Volcano vent from internal physical properties. Such considerations have been studied (see Calvache et al., 1997; Gil and Chouet, 1997) or are being researched.

Acknowledgments

The author wants to thank the strong help received from Greg Valentine from Los Alamos National Laboratory, whose advice and patience lets the author come to the equation system. Also to Bruno Martinelli (+) from ETHZ who always encouraged the author through his valuable criticism. And thanks to R.S.J Sparks from Bristol University, Augusto Neri from Consiglio Nazionale dele Ricerche and Omar Paredes from Universidad de Nariño for their valuable review of the previous manuscript. This research was supported by the Research System of the Universidad de Nariño, Colombia.

References

Banks, N., Calvache, M., Williams, S., 1997. c^{14} ages and activity for the past 50 ka at volcán Galeras, Colombia. Journal of Volcanology and Geothermal Research 77, 30–55.

Baxter, P., Neri, A., Todesco, M., 1995. Physical modeling and heat impact of pyroclastic flows. Periodico di Mineralogia 64, 95–97.

Betts, P., Sayma, A., 1993. Improved near ground treatment in finite element simulation of dense gas dispersion. Finite Elements in Fluids, New Trends and Applications, vol. 2. CIMNE, pp. 959–969.

Blong, R., 1984. Volcanic Hazards. Academic Press, Sidney, NSW.

Bursik, M., Woods, A., 1991. Bouyant, superbouyant and collapsing eruptions columns. Journal of Volcanology and Geothermal Research 45, 347–350.

Bursik, M., Woods, A., 1996. The dynamics and thermodynamics of large ash flows. Bulletin of Volcanology 58, 175–193.

Calvache, M., 1990. Geology and volcanology of the recent evolution of Galeras Volcano, Colombia. Master's thesis, Louisiana State Univ.

Calvache, M., 1995. The geological evolution of Galeras Volcanic complex. PhD thesis, Arizona State Univ.

Calvache, M., Cortés, G., Williams, S., 1997. Stratigraphy and chronology of the Galeras volcanic complex, Colombia. Journal of Volcanology and Geothermal Research 77, 5–19.

Chippada, R., Ramaswamy, B., Wheeler, M., Cowsar, L., Tetzlaff, D., 1993. Two-dimensional modeling of flow and sedimentation. Finite Elements in Fluids, New Trends and Applications, vol. 2. CIMNE, pp. 796–805.

Codina, R., Vazquez, M., Zienkiewicz, O., 1997. A General Algorithm for Compressible and Incompressible Flows. The Semi-Implicit Form. International Center for Numerical Methods in Engineering, Barcelona. Publication cimne 108.

Dobran, F., Neri, A., 1993. Numerical simulation of volcanic columns. Journal of Geophysical Research 98, 4231–4259.

Eguchi, Y., Yagawa, G., 1988. A large-scale three-dimensional finite element analysis of incompressible viscous fluid flow. Computational Mechanics 3, 241–254.

Espinoza, A., 1988. Actividad delvolcán Galeras en épocas históricas. Internal report. Ingeominas, Popayán, Colombia. In Spanish.

Fan, L., Zhu, C., 1998. Principles of Gas–Solid Flows. Cambridge University Press, Cambridge CB2 2RU.

Freunt, A., Bursik, M., 1998. Pyroclastic flow transport mechanisms. From Magma to Tephra. Elsevier, Amsterdam, pp. 173–245.

Gil, F., Chouet, B., 1997. Long period events, the most characteristic seismicity accompanying the emplacement and extrusion of a lava dome in Galeras volcano, Colombia, in 1991. Journal of Volcanology and Geothermal Research 77, 121–158.

Glowinski, R., Pironnean, O., 1992. Finite elements methods for Navier–Stokes equations. Annual Review of Fluid Mechanics 24, 167–204.

Gunn, D., 1978. Transfer of heat or mass to particles in fixed and fluidized beds. International Journal of Heat and Mass Transfer 21, 467–476.

Hartel, C., 1996. Turblent flows: direct numerical simulation and large-eddy simulation. Handbook of Computational Fluid Mechanics. Academic Press, pp. 283–338.

Hermann, F., Issler, D., Keller, S., 1994. Towards a numerical model of powder snow avalanches. Computational Fluid Dynamics '94. John Wiley and Sons, pp. 948–955.

Hurtado, A., Cortés, G., 1997. Third version of the hazard map of Galeras volcano, Colombia. Journal of Volcanology and Geothermal Research 77, 89–100.

Keller, S., 1996. Physikalische Simulation von Staublawinen: Experimente zur Dynamik im dreidimensionalen Auslauf. Ph.D. thesis. VAW der ETHZ, Zurich. In German.

Lai, W., Rubin, D., Krempl, E., 1974. Introduction to Continuum Mechanics. Pergamon Press, USA.

Larock, B., Schamber, D., 1981. Finite element computation of turbulent flows. Finite Elements in Water Resources. University of Missisippi, pp. 4.31–4.47.

Neri, A., Macedonio, G., 1996a. Numerical simulation of collapsing volcanic columns with particles of two sizes. Journal of Geophysical Research 101, 8153–8174.

Neri, A., Macedonio, G., 1996b. Physical modeling of collapsing volcanic columns and pyroclastic flows. Monitoring and Mitigation of Volcano Hazards. Springer-Verlag, pp. 389–427.

Neri, A., Macedonio, G., Gidaspow, D., Eposti Ongaro, T., 2001. Multiparticle Simulation of Collapsing Volcanic Columns and Pyroclastic Flows. Vsg report 2001-2. Instituto Nationale di Geofisica e Vulcanologia, Italy.

Sheridan, M., 1980. Pyroclastic block flow from the September, 1976 eruption of La Soufrière Volcano, Guadaloupe. Bulletin of Volcanology 43, 397–402.

Sparks, R., Wilson, L., 1976. A model for the formation of ignimbrite by gravitational column collapse. Journal of the Geological Society (London) 132, 441–451.

Sparks, R., Bursik, M., Carey, S., Gilbert, J., Glaze, L., Sigurdsson, H., Woods, A., 1997. Volcanic plumes. Pyroclastic Flows. Wiley, Chichester, pp. 141–179.

Sparks, R., Barklay, J., Calder, E., Herd, R., Komorowski, J., Luckett, R., Norton, G., Ritchie, L., Voight, B., Woods, A., 2002. Generation of a debris avalanche and violent pyroclastic density current on 26 December (boxing day) 1997 at Soufriere Hills volcano, Montserrat. In: Druits, T., Kokelaar, B. (Eds.), The Eruption of Soufriere Hills Volcano, Montserrat, from 1995 to 1999. Geological Society, London, vol. 21, pp. 409–434.

Stewart, H., Wendroff, B., 1984. Two-phase flow: models and methods. Journal of Computational Physics 56, 363–409.

Taniguchi, H., Suzuki-Kamada, K., 1993. Direct measurement of overpressure of a volcanic blast on June 1991 eruption at Unzen Volcano, Japan. Geophysical Research Letters 20, 89–92.

Taylor, C., Hughes, T., 1981. Finite Element Programming of the Navier–Stokes Equations. Pineridge Press Limited, UK.

Valentine, G., 1998. Damage to structures by pyroclastic flows and surges, inferred from nuclear weapons effects. Journal of Volcanology and Geothermal Research 87, 117–140.

Valentine, G., Wohletz, K., 1989. Numerical models of plinian eruptions columns and pyroclastic flows. Journal of Geophysical Research 94, 1867–1887.

Vazquez, M., Codina, R., Zienkiewicz, O., 1999. Numerical Modelling of Compressible Laminar and Turbulent Flow: The CBS Algorthm. Publication cimne 50. International Center for Numerical Methods in Engineering, Barcelona.

Wilcox, D., 1998. Turbulence Modeling for CFD. DWC Industries, USA.

Wohletz, K., 1998. Pyroclastic surges and compressible two-phase flow. From Magma to Tephra. Elsevier, Amsterdam, pp. 247–312.

Woods, A., Bursik, M., 1991. Particle fallout, thermal disequilibrium and volcanic plumes. Bulletin of Volcanology 53, 559–570.

Zienkiewicz, O., Codina, R., 1993. Search for a general fluid mechanics algorithm. Tech. Rep., vol. 44. CIMNE, Barcelona.

Zienkiewicz, O., Taylor, R., 1994. El método de los elementos finitos, vol. 2. CIMNE, Barcelona (in Spanish).